Antiviral Research 203 (2022) 105332

Contents lists available at ScienceDirect

Antiviral Research

journal homepage: www.elsevier.com/locate/antiviral

Development of a cost-effective ovine antibody-based therapy against SARS-CoV-2 infection and contribution of antibodies specific to the spike subunit proteins

Stephen Findlay-Wilson [a], Linda Easterbrook [a], Sandra Smith [b], Neville Pope [c], Gareth Humphries [d], Holger Schuhmann [d], Didier Ngabo [a], Emma Rayner [a], Ashley David Otter [a], Tom Coleman [a], Bethany Hicks [a], Victoria Anne Graham [a], Rachel Halkerston [a], Kostis Apostolakis [a], Stephen Taylor [a], Susan Fotheringham [a], Amanda Horton [a], Julia Anne Tree [a], Matthew Wand [a], Roger Hewson [a], Stuart David Dowall [a,*]

[a] United Kingdom Health Security Agency (UKHSA), Porton Down, Salisbury, Wiltshire, SP4 0JG, UK
[b] International Therapeutic Proteins Ltd (Australia), Longford, Tasmania, 7301, Australia
[c] International Therapeutic Proteins Ltd (UK), Goleigh Farm, Selborne, Hampshire, GU34 3SE, UK
[d] Native Antigen Company, Langford Locks, Kidlington, Oxford, OX5 1LH, UK

ARTICLE INFO

Keywords:
SARS-CoV-2
COVID-19
Antibodies
Therapy
Development
Omicron

ABSTRACT

Antibodies against SARS-CoV-2 are important to generate protective immunity, with convalescent plasma one of the first therapies approved. An alternative source of polyclonal antibodies suitable for upscaling would be more amendable to regulatory approval and widespread use. In this study, sheep were immunised with SARS-CoV-2 whole spike protein or one of the subunit proteins: S1 and S2. Once substantial antibody titres were generated, plasma was collected and samples pooled for each antigen. Non-specific antibodies were removed via affinity-purification to yield candidate products for testing in a hamster model of SARS-CoV-2 infection. Affinity-purified polyclonal antibodies to whole spike, S1 and S2 proteins were evaluated for *in vitro* for neutralising activity against SARS-CoV-2 Wuhan-like virus (Australia/VIC01/2020) and a recent variant of concern, B.1.1.529 BA.1 (Omicron), antibody-binding, complement fixation and phagocytosis assays were also performed. All antibody preparations demonstrated an effect against SARS-CoV-2 disease in the hamster model of challenge, with those raised against the S2 subunit providing the most promise. A rapid, cost-effective therapy for COVID-19 was developed which provides a source of highly active immunoglobulin specific to SARS-CoV-2 with multi-functional activity.

1. Introduction

The outbreak of coronavirus disease first identified in 2019 (COVID-19), caused by infection with the etiological agent severe acute respiratory syndrome coronavirus-2 (SARS-CoV-2), was declared a pandemic on March 11, 2020 (Cucinotta and Vanelli 2020). It continues to blight human public health, and the race to battle it with countermeasures continues apace. Whilst vaccines have made a valiant effort in the control of COVID-19, none of the current vaccines offer sterilising protection and there are major obstacles to overcome for global control of the virus (Kim et al., 2021). Therefore, new antiviral strategies will continue to play an important role in mitigating disease.

One of the first treatments explored early in the pandemic was antibody therapy sourced from previously infected patients. Convalescent human plasma was authorised for emergency use by the U.S. Food and Drug Administration (FDA) in August 2020 for the treatment of hospitalised patients with COVID-19. However, there are at least 176 registered clinical trials assessing convalescent plasma with seemingly contradictory results being reported (Piechotta et al., 2020; Ning et al., 2021). Major problems with convalescent plasma therapy include quality control and standardisation, defining optimal dosing and time-points and the risk of infection with unknown blood-borne infectious

* Corresponding author.
E-mail address: stuart.dowall@phe.gov.uk (S.D. Dowall).

https://doi.org/10.1016/j.antiviral.2022.105332
Received 20 December 2021; Received in revised form 29 April 2022; Accepted 3 May 2022
Available online 6 May 2022

agents (Ning et al., 2021). These issues can be overcome by using intravenous immunoglobulins (IVIG) which are sterile and purified from plasma collected from large pools of donors (Cao et al., 2020). However, the same issue applies with the reliance on human material as the source material.

As an alternative, animal-derived antibodies are more applicable for large scale production and standardisation. Ovine immunoglobulin G (IgG)-based products have been widely used as snake antivenoms (Gutierrez et al., 2011), and have been applied as treatments to infectious diseases including rabies (Redwan el, Fahmy et al. 2009) and tetanus (Redwan el, Khalil et al. 2005). The targeting of polyclonal antibodies to multiple epitopes enables a multitude of effector functions, such as steric hindrance (preventing the virus from attaching to the host cell surface), aggregation (bunching of viruses leading to clearance from the circulation), opsonisation (activation of phagocytic cells) and activation of the complement system (Haurum 2006).

We have previously applied the ovine polyclonal antibody-based approach to develop a cost-effective candidate against Ebola virus (EBOTAb) (Dowall et al., 2016), which demonstrated protection when given several days after challenge in the guinea pig (Dowall et al., 2016) and non-human primate (Dowall et al., 2017) disease models. Based on this success, it was appropriate to utilise this strategy to develop a similar therapy for COVID-19.

For the immunogens to develop the COVID-19 ovine antibody preparations, the full-length spike protein of SARS-CoV-2 was used alongside each of the two individual subunits. The spike protein controls SARS-CoV-2 infectivity with 30–40 spike homotrimers being present on the surface of each virion (Yao et al., 2020). Each spike protein has two subunits, S1 and S2. The S1 subunit contains the receptor-binding domain (RBD) which recognises the host cell receptor, angiotensin-converting enzyme 2 (ACE2) (Lan et al., 2020; Wang et al., 2020), whereas S2 mediates the sequential membrane fusion events allowing the virus to enter the host cytoplasm (Belouzard et al., 2012; Shang et al., 2020).

2. Materials and methods

2.1. Recombinant proteins

Full-length SARS-CoV-2 spike glycoprotein was produced in Chinese Hamster Ovary (CHO) cells with a His-tag incorporated (REC31868; Native Antigen Company, UK). Subunit SARS-CoV-2 S1 and S2 proteins were produced in human embryonic kidney cells (HEK293) with a sheep Fc-tag (REC31806 and REC31807, respectively; Native Antigen Company, UK).

2.2. Sheep

Border Leicester Cross Merino ewes of at least 12 months of age, born in Australia, were obtained from an approved supplier and kept at a controlled farm registered with the Australian Department of Agriculture. The farm operates under extremely high health status and standards of welfare, maintained by regular health inspections and veterinary checks which are carried out weekly and within 3 days of blood withdrawal.

2.3. Plasma and IgG production

Plasma and IgG production were conducted by International Therapeutic Proteins Ltd. Sheep were immunised on a 28 day schedule with 0.5 mg recombinant protein delivered subcutaneously across six sites: axillae (x2), groin (x2) and supra-scapula (x2). Six sheep were immunised with full-length spike glycoprotein and three for each of the S1 and S2 subunit proteins. Freunds Complete adjuvant was used for the first immunisation and Freunds Incomplete for subsequent ones. After a priming period that included two immunisations, plasma was collected via plasmapheresis using an automated MCS machine (Haemonetics Corporation, USA). Each collection typically yielded 600 ml plasma which was stored at −25 °C until further processing. Plasma was collected on a 28 day schedule, 2 weeks following immunisation alongside a 5 ml sera sample for assessing antibody levels at the time of collection. The IgG fraction was purified from the hyperimmune plasma by a series of polyethylene glycol (PEG) fractionations and a Zinc precipitation. The product was formulated at a concentration of 50–60 g/L in 20 mM Sodium Acetate/20 mM NaCl buffer.

2.4. Affinity-purification for candidate therapy manufacture

Affinity-purification of antibodies were undertaken by the Native Antigen Company. Columns were made using a ratio of ~5 mg recombinant protein per ~1g of de-hydrated, cyanogen bromide-activated Sepharose (Cytiva) according to manufacturer's instructions, resulting in 5 mL final resin per antigen. Unbound antigen was washed out with 3 × 2 column volumes (CV) of 0.1M NaOAc, pH4.0, 500 mM NaCl, followed by 3 × 2 CV of 0.1M Tris-HCl, pH8.0, 500 mM NaCl. This wash cycle was repeated twice. For the purification of antibodies, the resins were transferred to 10 mL polypropylene gravity flow columns (ThermoFisher).

The PEG precipitated IgG-fraction was pH-adjusted by the addition of 1M HEPES, pH8.0 (1.25 mL per 10 mL of original IgG fraction). After centrifugation (10 min, 4000×*g*, 20 °C), the clarified supernatant was loaded on the respective antigen column equilibrated in 10 mM HEPES pH 8.0 with a contact time of approx. 1.5 h. The columns were washed with 10 CV of equilibration buffer, followed by 10 CV 10 mM HEPES pH 8.0, 300 mM KCl. Antibodies were eluted with 100 mM glycine, pH 2.5. Protein containing fractions were pooled and adjusted to pH7-8 with 1M Tris-HCl, pH9.0 (1/5th of the original volume) before dialysis into DPBS.

2.5. Enzyme-linked immunosorbent assay

Nunc MaxiSorp microtitre plates were coated with 2 μg/ml recombinant protein in bicarbonate buffer overnight at 2–8 °C. Plates were washed 3 times with phosphate buffered saline (PBS) containing 0.05% Tween20 (PBST) and blocked for 1 h at 37 °C with blocking buffer (5% skimmed milk powder in PBS). Plates were incubated for 1 h at 37 °C with prediluted samples (sera collected from sheep bleeds or purified antibody preparations); washed with PBST; and incubated with a donkey anti-ovine IgG horseradish peroxidase (HRP) conjugate (Product 713-035-003; Jackson ImmunoResearch, USA) for 1 h at 37 °C. After further washing, TMB substrate was added and the reaction was stopped by the addition of stop solution before reading the optical density at a wavelength of 450 nm.

2.6. Receptor binding domain (RBD) binding assay

Anti-RBD antibodies were determined using the fully quantitative Roche Elecsys anti-SARS-CoV-2 S assay (ACOV2 S), a species independent electrochemiluminescent immunoassay (ECLIA). Samples are considered negative if < 0.8 U/ml, or positive if > 0.8 U/ml, with a detection range of 0.400–225,000 U/ml.

2.7. Neutralisation assay

SARS-CoV-2 Australia/VIC01/2020 (GISAID accession, EPI_ISL_406844) (Caly et al., 2020) was generously provided by The Doherty Institute, Melbourne, Australia and was subsequently passaged in Vero/hSLAM cells [ECACC 04091501] (European Collection of Cell Cultures, UK) to produce a working stock at passage 4 (P4), at the UKHSA, Porton Down, UK. Whole genome sequencing was performed on the P4 stock, using SISPA amplification on both Nanopore and Illumina technologies as described previously (Lewandowski et al., 2019). SARS-CoV-2 lineage B.1.1.529 BA.1 (Omicron) was isolated at UKHSA,

Porton Down from a nasopharyngeal swab taken from a UK patient. Whole genome sequencing was performed on the P2 stock (HCM/V/127) used in this assay (GenBank: OM003685).

A micro-neutralisation assay based on a previously published protocol (Bewley et al., 2021), with minor modifications, was used to assess the neutralising activity of the antibodies. Antibodies were diluted 2-fold over a 12-step dilution range (50 μg/ml – 0.02 μg/ml), in duplicate (technical replicates). A fixed concentration of SARS-CoV-2 was added to the diluted antibody. Additional assay wells included virus-free and untreated virus-only controls. The neutralising plates (diluted antibody & virus) were then incubated for 1 h at 37 °C, afterwards the contents were then transferred onto 96-well plates containing Vero-E6 cells (ECACC 85020206) and the virus was allowed to adsorb to the cells for 1 h at 37 °C. The inocula were removed from the wells before the addition of 100 μl overlay media (MEM containing 4% FCS and 1% carboxymethylcellulose (CMC) solution) to each well. Plates were incubated for 24h (Victoria isolate) or 26h (Omicron BA.1) at 37 °C to allow foci to form.

After incubation cells were fixed overnight with 8% (w/v) formalin/PBS, washed with water and permeabilised with 0.2% (w/v) Triton X-100/PBS at room temperature for 10 min. Cells were washed with PBS, incubated with 0.3% hydrogen peroxide (Sigma) at room temperature for 20 min and washed with PBS. Foci were stained with 50μl/well rabbit anti-nucleocapsid (Sino Biological, 40588-T62) diluted 1:1000 in 0.2% (w/v) Triton X-100/PBS for 1 h at room temperature. Antibody dilutions were discarded, cells washed with PBS and incubated with 50μl/well goat anti-rabbit IgG HRP (Invitrogen, G-21234) diluted 1:4000 in 0.2% (w/v) Triton X-100/PBS for 1h at room temperature. Cells were washed with PBS and incubated with TrueBlue peroxidase substrate (SeraCare, 5510-0030) for 10 min at room temperature then washed with water. Infectious foci were counted with an ImmunoSpot® S6 Ultra-V 367 analyser with BioSpot counting module (Cellular Technologies Europe, Germany). The counted foci data were then imported into R- Bioconductor. Two or three independent experiments were performed for each antibody. The internal positive control for the Victoria isolate was convalescent plasma, donated to UKHSA from the Northern Ireland Blood Transfusion Service (NIBTS), from a patient recovering from a Wuhan-like virus. The internal positive control for the Omicron BA.1 variant was convalescent plasma, donated to UKHSA, from a patient recovering from Omicron infection.

A midpoint probit analysis (written in R programming language for statistical computing and graphics) was used to determine the amount (μg/mL) of antibody required to reduce SARS-CoV-2 viral foci by 50% (IC_{50}) compared with the virus only control (n = 10).

2.8. Antibody-dependent complement deposition (ADCD) assay

SPHERO carboxyl magnetic blue fluorescent beads (Spherotech, USA) were coupled with SARS-CoV-2 whole spike protein (Lake Pharma, 46328) using a two-step sulpho-NHS/EDC process detailed by Brown et al., (2012) (Brown et al., 2012). Spike protein was included at saturation levels and coupling confirmed by the binding of IgG from a COVID-19 convalescent donor known to have high levels of anti-spike protein IgG. Heat-inactivated NIBSC Anti-SARS-CoV-2 Antibody Diagnostic Calibrant (NIBSC, 20/162) at an initial 1:40 dilution (10 μl sera into 30 μl blocking buffer (BB; PBS, 2% bovine serum albumin (BSA)) followed by a 1:10 dilution into BB) with an assigned arbitrary unitage of 1000U/ml was added in duplicate and serially diluted 2:3 in BB. Affinity-purified ovine polyclonal antibodies (3 μl in duplicate) were added to 27 μl BB and serially diluted 1:3 in BB. This was followed by 20 μl of SARS-CoV-2 spike protein-coated magnetic beads (50 beads per μl) to give a final 1:3 serial dilution range starting at 1:20. The serial dilution for NIBSC 20/162 standard started at 1:80. The mixture was incubated at 25 °C for 30 min with shaking at 900 r.p.m. The beads were washed twice in 200 μl wash buffer (BB+0.05% Tween-20), then resuspended in 50 μl BB containing 10% IgG- and IgM-depleted human plasma (prepared per (Alexander et al., 2022)) and incubated at 37 °C for 15min with shaking at 900 r.p.m. Beads were next washed twice with 200 μl wash buffer and resuspended in 100 μl fluorescein (FITC)-conjugated rabbit anti-human C3c polyclonal antibody (Abcam) diluted 1:500 in BB and incubated in the dark. After two more washes with 200 μl wash buffer, the samples were resuspended in 40 μl HBSS and analysed using an iQue Screener Plus® with iQue Forecyt® software (Sartorius, Germany). For each sample, a minimum of 100 beads were collected. Conjugated beads were gated based on forward scatter and side scatter and then further gated by allophycocyanin (APC) fluorescence. The APC fluorescent-bead population was gated and measured for FITC Median Fluorescent Intensity, which represents deposition of C3b/iC3b (gating strategy shown in Supplementary Fig. 1). The NIBSC 20/162 calibrant was plotted as a 4 parameter logistic (PL) curve with 1/Y2 weighting and the linear range calculated. The mean fluorescence intensity (MFI) from each sample was interpolated against the NIBSC 20/162 4 PL curve and the calculated concentration that hit the linear range was multiplied by the dilution factor to assign activity of the sera as Complement Activating Units (CAU).

2.9. Antibody-dependent neutrophil phagocytosis (ADNP) assay

1 μm crimson-fluorescent carboxylate-modified FluoSpheres™ (Thermo Fisher, F8816) were coupled with SARS-CoV-2 whole spike protein (Lake Pharma, 46328) using a two-step sulpho-NHS/EDC process detailed by Brown et al., (2012) (Brown et al., 2012). In a 96-well round bottom microtitre plate (Thermo Scientific; 612U96), 20 μL of pre-diluted (ten-point serial dilution from 1:20 to 1:10,240) samples or anti-SARSCoV-2 antibody diagnostic calibrant reagent (NIBSC; 20/162) were mixed with 20 μL of DPBS-GACM buffer (Dulbecco's PBS supplemented with 0.1% w/v glucose, 0.5% w/v BSA, 0.9 mM $CaCl_2$ and 0.5 mM $MgSO_4$ at pH 7.4) containing one million beads. The mix was incubated for 30 min at 37 °C, with shaking at 900 rpm, before the addition of 20 μL of 1:10 diluted IgM- and IgG-depleted human plasma (Alexander et al., 2022) and 40 μL of DPBS-GACM containing 2.5×10^6/ml granulocyte-differentiated HL-60 cells (ATTC; CCL-240, differentiated with 0.8% N,N-dimethylformamide for 5 days). The plate was incubated for 30 min at 37 °C with shaking at 900 rpm and phagocytosis stopped by placing the plate on ice and adding 80 μL of cold DPBS with 0.02% EDTA. Samples were analysed using an iQue Screener Plus® with iQue Forecyt® software (Sartorius, Germany). Units were quantified by interpolating the MFI of test samples from a 4 PL standard curve of the NIBSC 20/162 calibrant (designated to have 1000 units of anti-SARS-CoV-2 opsonophagocytic activity; gating strategy shown as Supplementary Fig. 2).

2.10. MSD assay

Samples were determined for their capability at neutralising different variants of concern using the MesoScale Discovery ACE2 assays. Samples were run using the MSD Plate 13 (K15466U) which harbours full-length spike antigens specific to Wuhan and 9 different VOC: Alpha (B.1.1.7), Beta (B.1.351), Gamma (P.1), Delta (B.1.617.2), Zeta (P.2), Kappa (B.1.617), B.1.617.3, B.1.526.1 and B.1.617.1. Samples were incubated according to the manufacturer's instructions. Results are reported in neutralising antibodies (μg/ml).

2.11. Hamsters

Golden Syrian hamsters, aged 7–9 weeks (weight range 122–162g), were obtained from a UK Home Office accredited facility (Envigo RMS UK Ltd). Animals were housed in cages in accordance with the requirements of the UK Home Office Code of Practice for the Housing and Care of Animal Used on Scientific Procedures (1986). During procedures with SARS-CoV-2 animals were housed in a flexible-film isolator within a Containment Level 3 facility. Animals were randomly put into groups,

with equal allocation of male and female animals. Group sizes of 6 hamsters were used as the minimal number required for statistical significance to be achieved. Access to food and water was *ad libitum* and environment enrichment was provided. All experimental work was conducted under the authority of a UK Home Office approved project licence that had been subject to local ethical review at Public Health England (now part of the UK Health Security Agency (UKHSA)) Porton Down by the Animal Welfare and Ethical Review Body (AWERB) as required by the Home Office Animals (Scientific Procedures) Act 1986. Humane clinical endpoints consisted of 20% weight loss or severe signs of disease/distress, with animals reaching these limits being culled.

2.12. Antibody administration

Affinity-purified antibodies were administered to hamsters after diluting to a concentration of 1 mg/mL with PBS and injecting 2 mL via the intraperitoneal route. On the day before challenge, four groups of hamsters received therapy: antibodies to whole spike, S1 and S2 proteins or PBS control. A separate group received antibodies to whole spike protein on day 3 post-challenge.

2.13. Virus challenge

SARS-CoV-2 Victoria/01/2020, described earlier, was used at passage 3. Challenge dilutions were made in sterile PBS with delivery via intranasal instillation (200 μL total with 100 μL per nare).

2.14. Clinical observations

Animals were monitored for abnormal clinical signs twice daily. These were assigned a score based upon the following criteria: 0, normal; 1, behavioural changes; 2, ruffled fur, dehydrated, wet tail; 3, arched, wasp-waisted, eyes shut; and 5, laboured breathing. At the same time each day, animals were weighed.

2.15. Sampling

Pharyngeal swabs were taken on day 2, 4, 6, 8 and 9 post-challenge. A dry flocked mini-tip swab (product MW002NF; MWE, UK) was used for sampling before adding to 1 mL Virocult universal transport media (product MW951T; MWE, UK). On day 2 post-challenge, a nasal wash was conducted by instillation of 200 μL PBS into each nare with a flexible feeding tube and collection of fluid extract.

At the end of the study, animals were anaesthetised with isoflurane followed by a lethal dose of sodium pentobarbitone delivered via the intraperitoneal route. During necropsy, a sample of lung was collected for molecular analysis. The thoracic pluck (consisting of lung, trachea and associated structures) and the head were immersed in 10% neutral-buffered formalin for histological examination.

2.16. Focus-forming unit (FFU) assay

Pharyngeal swab and nasal wash samples collected at day 2 were quantified for live virus using a FFU assay. Samples were serially diluted before adding, in duplicate, to a VeroE6 cell monolayer in a 96-well flat bottomed culture plates (seeded 24 h before) for 1 h at 37 °C. Samples were removed and overlay media added, then incubated for 24 h at 37 °C. Plates were fixed overnight by adding 20% formalin and then fumigated before staining using the same techniques as for the neutralisation assay.

2.17. Quantification of viral loads by RT-qPCR

Samples from pharyngeal swabs and lung homogenates were RNA extracted using the BioSprint one-for-all vet kit (Indical, UK) and Kingfisher Flex platform (ThermoFisher, UK). Reverse transcription-quantitative polymerase chain rection of the nucleocapsid (N) gene was used to determine viral loads and was performed using TaqPath™ 1-Step RT-qPCR Master Mix, CG (Applied Biosystems™), 2019-nCoV CDC RUO Kit (Integrated DNA Technologies) and QuantStudio™ 7 Flex Real-Time PCR System. Sequences of the N1 primers and probe were: 2019-nCoV_N1-forward, 5′ GACCCCAAAATCAGCGAAAT 3'; 2019-nCoV_N1-reverse, 5′ TCTGGTTACTGCCAGTTGAATCTG 3'; 2019-nCoV_N1-probe, 5′ FAM-ACCCCGCATTACGTTTGGTGGACC-BHQ1 3', targeting a region of the SARS-CoV-2 nucleocapsid. The cycling conditions were: 25 °C for 2 min, 50 °C for 15 min, 95 °C for 2 min, followed by 45 cycles of 95 °C for 3 s, 55 °C for 30 s. The quantification standard was *in vitro* transcribed RNA of the SARS-CoV-2 N ORF (accession number NC_045512.2) with quantification between 1 × 10e1 and 1 × 10e6 copies/μl.

2.18. Pathological studies

The left lung lobe and a sagittal section of the entire nasal cavity were fixed by immersion in 10% neutral-buffered formalin, processed and embedded into paraffin wax. The nasal cavity was decalcified using an EDTA-based solution prior to embedding. Sections of 4 μm were cut and stained with hematoxylin and eosin (HE) and examined microscopically. In addition, samples were stained using the RNAscope technique to visualise SARS-CoV-2 virus RNA. Briefly, tissues were pretreated with hydrogen peroxide for 10 min (room temperature), target retrieval for 15 min (98–101 °C) and protease plus for 30 min (40 °C) (Advanced Cell Diagnostics). A V-nCoV2019-S probe (Cat No. 848561, Advanced Cell Diagnostics) was incubated on the tissues for 2 h at 40 °C. Amplification of the signal was carried out following the RNAscope protocol using the RNAscope 2.5 HD Detection kit – Red (Advanced Cell Diagnostics).

All slides were scanned digitally using a Hamamatsu S360 digital slide scanner and examined using ndp.view2 software (version 2.8.24). Sections were examined by a qualified veterinary pathologist who was blinded to the animal and treatment groups. A semi-quantitative histopathology scoring system was used to evaluate microscopic lesions in the lung and nasal cavity (reported elsewhere (Dowall et al., 2021)); in addition, 'Nikon NIS-Ar' software (version 5.21.02) was used to perform digital image analysis to calculate the percentage area of pneumonia and quantify the presence of viral RNA in lung sections. For nasal cavity, a semiquantitative scoring system was applied to evaluate the presence of virus RNA: 0 = no positive staining; 1 = minimal; 2 = mild; 3 = moderate and 4 = abundant staining.

2.19. Statistical analysis

Statistical analyses were performed using MiniTab, version 16.2.2 (Minitab Inc). A non-parametric Mann-Whitney statistical test was applied to ascertain significance between groups. A significance level below $P = 0.05$ was considered statistically significant.

3. Results

3.1. Seroconversion of immunised sheep

All sheep immunised with recombinant SARS-CoV-2 proteins exhibited strong antibody responses with the 1st sample collected after two immunisations (Fig. 1). Following subsequent monthly immunisations, the titres were maintained at equivalent high levels. Plasma collected at all of the timepoints were therefore pooled and purified to produce stocks of purified IgG.

3.2. Binding of purified antibody preparations to whole spike protein and subunits

Purified IgG pooled from plasmapheresis events was tested alongside

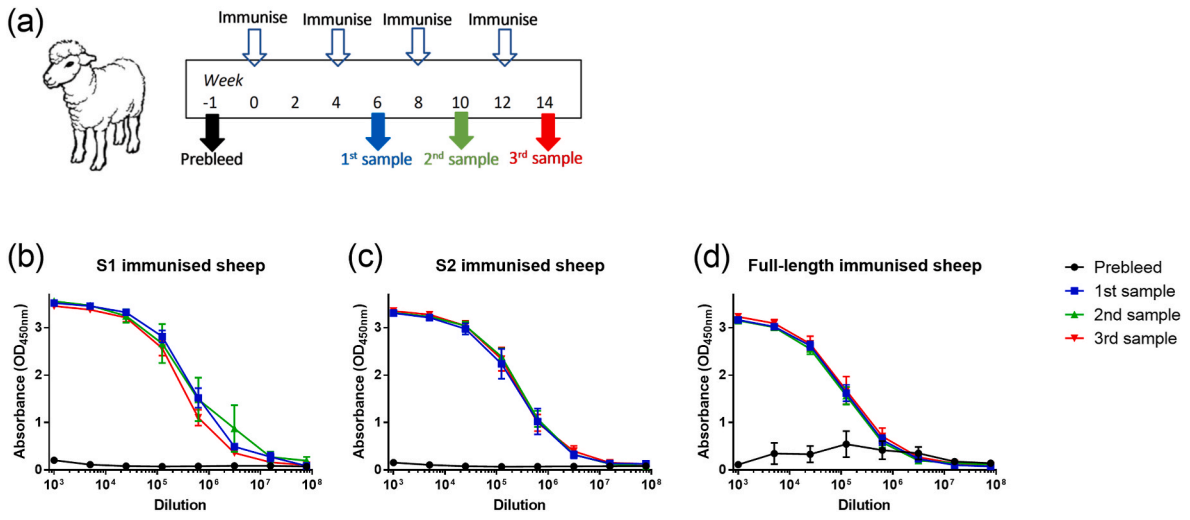

Fig. 1. Binding of ovine sera to full-length recombinant SARS-CoV-2 spike protein after immunisation with glycoprotein antigens. (a) Outline of study schedule. (b) Reactivity of S1-immunised sheep, n = 3. (c) Reactivity of S2-immunised sheep, n = 3. (d) Reactivity of full-length immunised sheep, n = 6. Lines show mean values with error bars denoting standard error.

antibody preparations that had been affinity-purified to remove non-specific antibodies. Antibodies generated in response to immunisation with full-length spike proteins and the S1 or S2 subunits all recognised recombinant whole spike protein (Fig. 2a). As expected, antibodies generated from sheep immunised with S2 antibodies produced low levels of S1-specific responses (Fig. 2b) and similarly S1-derived antibodies demonstrated low responses to S2 antigen (Fig. 2c). The affinity-purified preparations consistently gave higher binding compared to the parent purified antibody preparations.

3.3. Functional activity of affinity-purified antibodies

Antibodies were tested for their ability to neutralise live viral strains from early in the pandemic (Wuhan-like virus, Victoria) and a recent divergent strain (Omicron BA.1 variant). The antibody raised against the full-length spike protein demonstrated the greatest neutralisaing activity against the Wuhan-like virus with an IC50 value of 49 ng/ml.

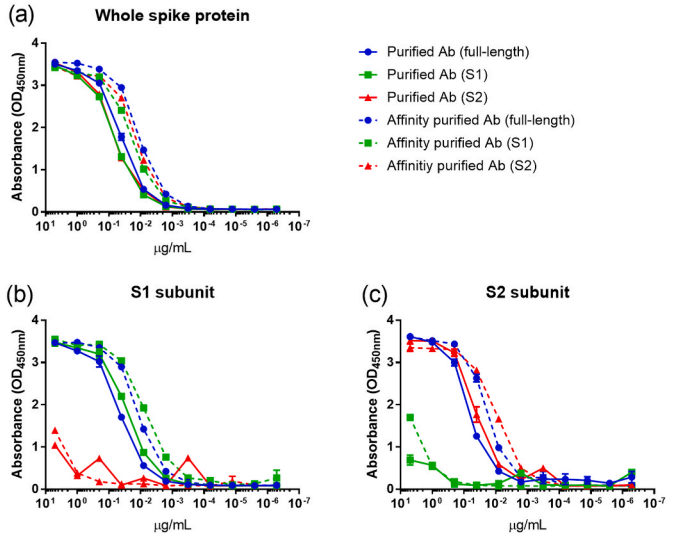

Fig. 2. Antigen binding kinetics of purified and affinity-purified IgG preparations to recombinant SARS-CoV-2 glycoproteins. (a) Reactivity to whole spike protein. (b) Reactivity to S1 subunit protein. (c) Reactivity to S2 subunit protein. Lines show mean values. Solid line, purified antibodies; dashed line, affinity-purified antibodies.

Antibodies raised against the S1 and S2 spike protein also had neutralising activity with IC_{50} values of 1.071 and 0.428 µg/ml respectively (Table 1). All preparations had strong neutralisation activity to both SARS-CoV-2 strains, although ~10-fold higher antibody concentrations were required to neutralise the Omicron BA.1 variant.

To determine the breadth of *in vitro* activity of antibodies, a range of tests were undertaken. Firstly, binding specific to the receptor-binding site was assessed, with both the full-length and S1-specific antibodies demonstrating strong recognition, whereas the S2-specific antibody did not bind (Fig. 3a). Antibody-dependent complement deposition was observed with all three antibody preparations, with lower but similar levels observed for S1- and S2-specific preparations compared to those derived from sheep immunised with full-length spike protein (Fig. 3b). Using an antibody-dependent neutrophil phagocytosis assay, the full-length produced antibodies had higher activity than S1-derived antibodies, whereas the S2-derived antibodies were less opsonophagocytotic (Fig. 3c). Antibodies raised against the full-length spike protein reacted strongly to the RBD and spike antigens from different SARS-CoV-2 variants, including alpha (B.1.1.7), beta (B.1.351) and gamma (P.1),

Table 1
Neutralisation activity of two divergent strains of SARS-CoV-2 by ovine antibody preparations. IC_{50} values from 2 to 3 independent experiments with 95% confidence intervals around the probit midpoint (IC_{50}) and overall geometric mean IC_{50}.

SARS-CoV-2 strain	Antibody preparation	Neutralisation activity probit midpoint(IC_{50}) µg/ml (95% confidence interval)	Geometric mean IC_{50} µg/ml
Victoria Wuhan-like virus	Full-length	0.067 (0.061–0.074) 0.061 (0.054–0.069) 0.028 (0.023–0.032)	0.049
	S1 subunit	1.349 (1.120–1.625) 1.011 (0.461–2.212)	1.071
	S2 subunit	0.934 (0.731–1.192) 0.196 (0.08–0.383)	0.428
Omicron B.1.1.529 BA.1	Full-length	0.322 (0.246–0.420) 0.545 (0.414–0.716) 1.485 (0.948–2.344)	0.639
	S1 subunit	21.794 (20.044–23.710) 18.789 (5.509–284.044) 14.833 (6.25–64.298)	18.246
	S2 subunit	59.039 (30.853–211.856) 10.509 (6.167–21.208) 3.258 (0.422–655.149)	5.851

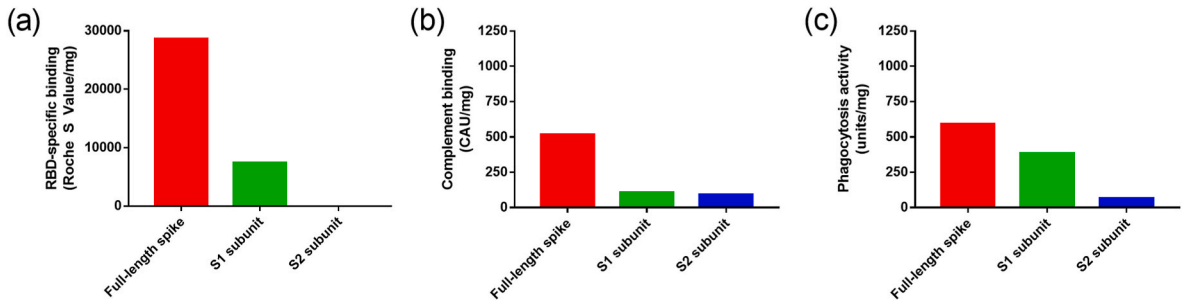

Fig. 3. Functional activity of affinity-purified antibodies produced against recombinant SARS-CoV-2 glycoproteins. (a) Binding to the SARS-CoV-2 RBD. Bars show mean values with error bars denoting standard error from triplicate samples. (b) Antibody-dependent complement deposition. (c) Antibody-dependent neutrophil phagocytosis. Results from a single assay are shown. (b–c) Data is calibrated to the NIBSC 20/162 SARS-CoV-2 antibody diagnostic calibrant consisting of a pool of convalescent plasma from 3 separate donors and assigned a unitage of 1000 units/ml.

whereas the S1-raised preparation cross-reacted only with the RBD of the variants, and S2 showed limited cross-reactivity (Table 2). The level of interaction of the two subunit antibody preparations were consistently lower than those observed with the full-length preparation, with the S2 antibodies only reaching inhibition levels of 50.7% and below.

3.4. Protective effect of affinity-purified antibodies against SARS-CoV-2 disease in hamsters

To assess the ability of antibodies to protect against SARS-CoV-2 disease, hamsters received 2 mg antibody 24 h before challenge. In addition, a further group received antibodies specific for full-length spike protein 3 days post-challenge for therapeutic effect. Results demonstrated that in comparison to a PBS control group, hamsters that received the antibodies lost less weight, with the groups that received full-length or S2 specific antibodies showing no evidence of any weight loss (Fig. 4a). When the maximum weight loss of individual animals was analysed, all control animals lost weight, whereas weight loss in other groups was less marked (Fig. 4b). The differences between the PBS group and the full-length and S2 groups were statistically significant ($P = 0.0202$ and 0.0051, respectively) whereas significance was not reached for the S1 and delayed full-length treated groups ($P = 0.0656$ and 0.2623, respectively). The clinical score of animals which received either the full-length spike, S1 subunit and S2 subunit antibodies were markedly lower than the PBS control group (Fig. 4c). Observations in the S2 subunit group were only the minimal sign of ruffled fur which was seen in two animals. In the PBS control group, three animals met humane endpoints during the course of the study; but this difference was just outside of statistical significance ($P = 0.056$, Log-Rank survival test).

Table 2
Recognition of antigens from SARS-CoV-2 variants by ovine antibody preparations.

	Ovine antibody preparation		
	Full-length	S1 subunit	S2 subunit
SARS-CoV-2 RBD (B.1.1.7)	99.197	78.347	2.180
SARS-CoV-2 RBD (P.1)	97.214	75.465	14.960
SARS-CoV-2 S1 RBD	99.757	84.056	13.977
SARS-CoV-2 S1 RBD (B.1.351)	98.309	87.894	50.711
SARS-CoV-2 Spike	99.795	58.721	49.074
SARS-CoV-2 Spike (B.1.1.7)	98.831	26.369	22.948
SARS-CoV-2 Spike (B.1.351)	95.801	18.956	30.435
SARS-CoV-2 Spike (P.1)	96.395	20.529	35.644

Data show percentage inhibition of ACE2 binding using a MesoScale Discovery assay with each antibody preparation being standardised to a concentration of 1 mg/ml.

3.5. Antibody levels at time of challenge

Prior to challenge, a blood sample was collected to enable the concentration of circulating antibody to be evaluated. Results showed that in the full-length spike and S1 subunit groups, one animal had low amounts of antibodies (Fig. 5a). To determine whether this was the cause of a failure to protect against disease, a correlation was plotted with the maximum weight loss which demonstrated that the animals with low ovine-specific antibody concentrations were those which showed a more severe clinical disease (Fig. 5b).

3.6. Effects of antibody preparations on viral loads in hamsters after SARS-CoV-2 challenge

Nasal wash and a pharyngeal swab were collected 2 days post-challenge to assess the levels of live SARS-CoV-2. In animals which received antibody treatment prior to challenge, there were lower levels of live virus in the nasal wash and pharyngeal swabs samples (Fig. 6a); however, these did not reach statistical significance with the full-length group being the closest in the nasal wash sample ($P = 0.0782$, Mann-Whitney test). Pharyngeal swabs were collected at regular times throughout the study and tested for the presence of viral RNA. Levels remained similar across animals who received antibodies compared to the PBS control group until day 8, where significantly lower levels of viral RNA were detected in the animals which received antibodies raised to the S2 subunit ($P = 0.0282$ on day 8 and 9 timepoints, Mann-Whitney test) (Fig. 6b). At necropsy, viral RNA levels in the lung were assessed with levels in the PBS control animals which met humane clinical endpoints were higher than those which survived to the scheduled end of the study (Fig. 6c); these were excluded from statistical comparison with the groups which received antibodies due to samples being collected at a different timepoint. Viral RNA levels in the lungs were lower in several animals in the groups that received antibody compounds prior to challenge, reaching significance in the S2 subunit group ($P = 0.0282$, Mann-Whitney test).

3.7. Histopathological changes in hamsters given ovine antibody preparations after challenge with SARS-CoV-2

Lesions consistent with infection with SARS-CoV-2 were observed within the left lung lobe and nasal cavity in animals in both the treated groups and the control group. Lung lesions consisted of a multifocal to coalescing broncho-interstitial pneumonia with areas of consolidation. Inflammatory cells, primarily macrophages and neutrophils with some lymphocytes and plasma cells, infiltrated alveolar walls and filled alveolar spaces, with cell degeneration and loss, and patchy alveolar oedema; prominent type II alveolar hyperplasia was noted in some areas. The airways were also infiltrated by similar inflammatory cells. Whilst the bronchi contained fewer inflammatory cells, changes in

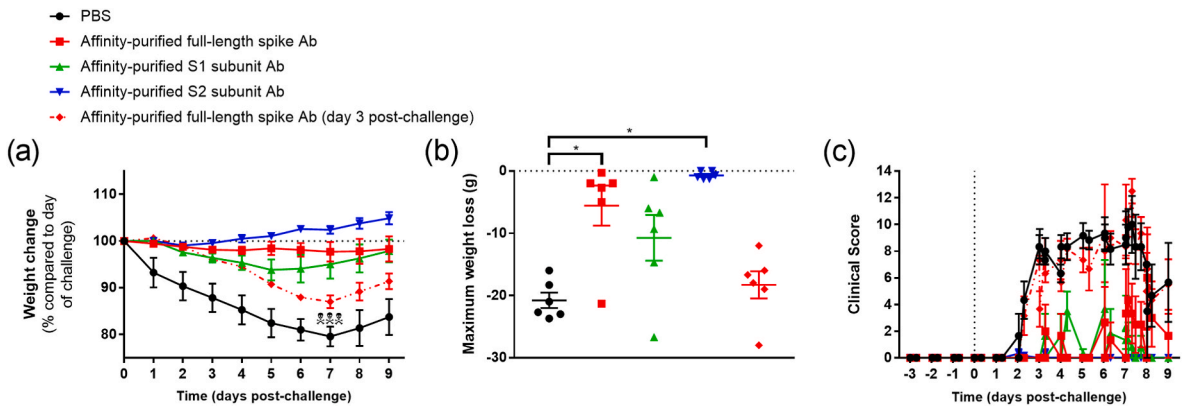

Fig. 4. Clinical outcomes of hamsters receiving antibody preparations after challenge with SARS-CoV-2. (a) Weight of animals. Lines show mean value with error bars denoting standard error. Dotted line shows day of challenge. Three animals in the PBS group met humane clinical endpoint as indicated by skull and crossbones symbol. (b) Maximum weight loss of animals, with line and whisker plots showing mean value and standard error. (c) Clinical score. Lines show mean values with error bars denoting standard error. . n = 6 hamsters per group.

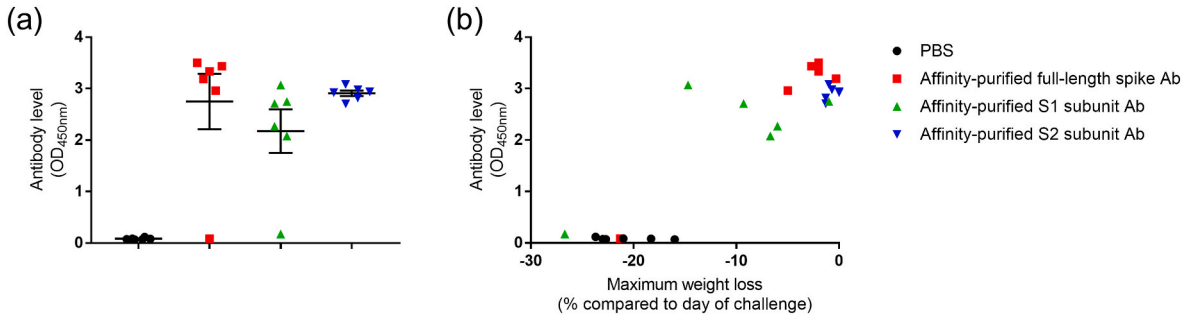

Fig. 5. Antibody levels on day of challenge and comparison to subsequent weight loss. (a) Antibody levels from sera collected on the day of challenge. Results show mean absorbance level from duplicate wells from each animal tested at a 1:100 dilution. Bar and whisker plots denote mean and standard error. (b) Comparison of animal level at time of challenge with maximal weight loss observed after challenge with SARS-CoV-2. n = 6 hamsters per groups.

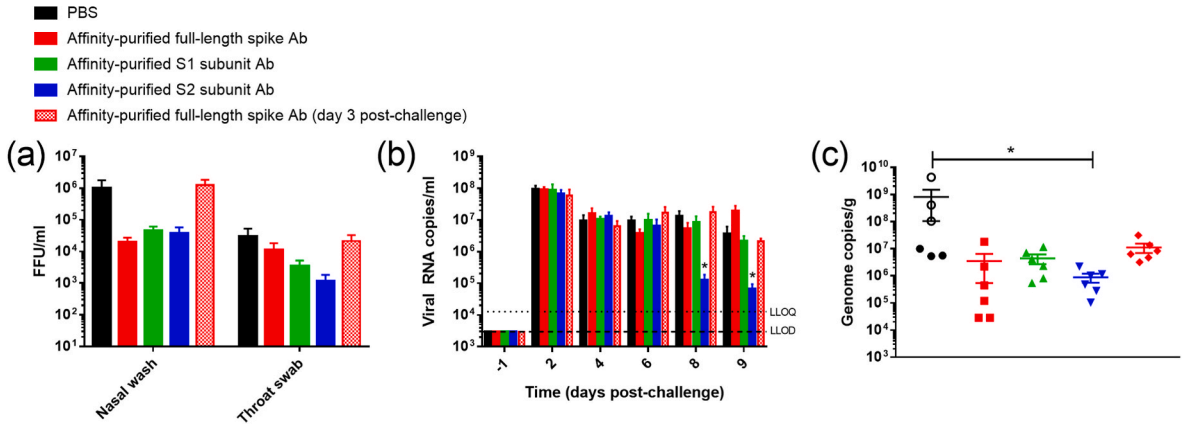

Fig. 6. Virology readouts of hamsters receiving ovine antibody preparations after challenge with SARS-CoV-2. (a) Quantification of live virus detected by focus-forming assay in nasal wash and pharyngeal swab samples collected 2 days post-challenge with SARS-CoV-2. Bars show mean values with error bars denoting standard error. No statistical significance between groups receiving antibodies compared to PBS control ($P > 0.05$). (b) Viral RNA levels in pharyngeal swabs. Bars show mean values with error bars denoting standard error. *, $P < 0.05$. (c) Viral RNA levels in lung tissue collected at necropsy. Open circles indicate animals which met humane clinical endpoints. Individual results shown with line and whisker plots showing mean value and standard error. *, $P < 0.05$.

bronchioles, particularly at the bronchioloalveolar junctions, were of increased severity, with concomitant epithelial cell degeneration and loss. Bronchi and bronchioles were surrounded variably by lymphocytes and other inflammatory cells. Lymphocytes were also noted surrounding blood vessels and occasionally infiltrating the walls. The lesions in the nasal cavity were characterised by presence of exudates (fluid with inflammatory cells, mainly neutrophils but also mononuclear cells) and degeneration and necrosis of the epithelium in the respiratory and olfactory mucosa. Representative images of microscopic changes are shown in Fig. 7.

Overall, lesion severity was significantly less in the lung of animals given full-length and S2 ovine antibodies compared to those receiving the negative control ($P = 0.0374$ and $P = 0.0163$, respectively, Mann-Whitney test) (Fig. 8b). Furthermore, the percentage of consolidation

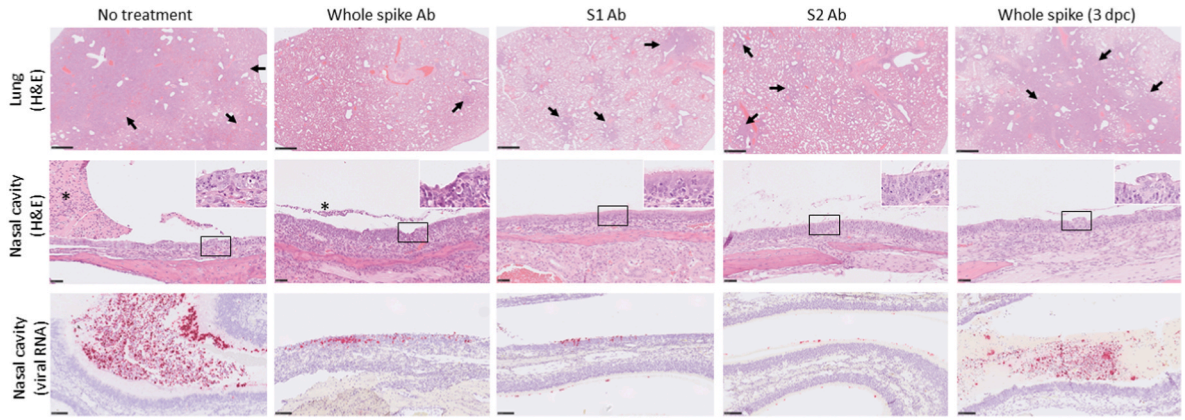

Fig. 7. Representative microscopic images of lungs and nasal cavities of hamsters receiving ovine antibody preparations after challenge with SARS-CoV-2. Top row, lung-multifocal to patchy areas of pneumonic consolidation (arrows) (H&E); middle row, nasal cavity-inflammation and degeneration of the mucosa with variable luminal exudate (asterisks). Inset, higher power images of nasal epithelium (×800 magnification) (H&E); lower row, nasal cavity-staining for SARS-CoV-2 viral RNA in the mucosa and luminal exudate (*in situ* hybridisation).

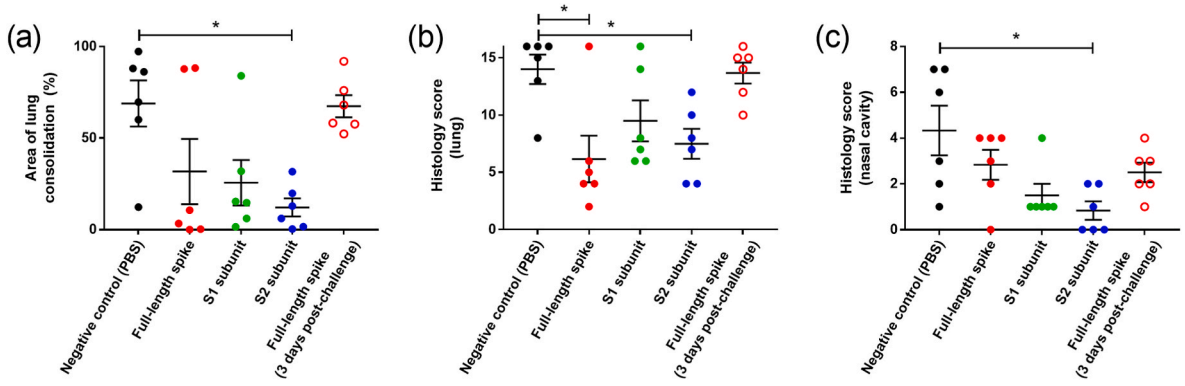

Fig. 8. Pathological readouts in the lungs and nasal cavities of hamsters receiving ovine antibody preparations after challenge with SARS-CoV-2. (a) Area of consolidation in the lung as a percentage. (b) Total pathology score in the lung. (c) Total pathology score in the nasal cavity. Line and whisker plots show mean value and standard error. *, $P < 0.05$.

in the lung, which represented the severity of pneumonic change, was reduced in the S2 antibody group and reached statistical significance ($P = 0.0202$, Mann-Whitney test) (Fig. 8a). In the nasal cavity, a reduction in lesion severity only reached significance in the S2 ovine antibody group ($P = 0.0250$, Mann-Whitney test) (Fig. 8c). Whilst the histological outcomes in the S2 antibody group were significant across the different analysis, the results demonstrate lower levels of lung consolidation and histological scores in many of the animals which received antibody treatment prior to challenge, indicating an effect in the majority of animals but little effect when administration was delayed to 3 days post-challenge (Fig. 8a–c).

4. Discussion

Our work has established proof-of-concept evidence that hyperimmune ovine immunoglobulins can confer protective effects against SARS-CoV-2 infection using a stringent preclinical animal model. Antibodies were raised against three antigens: whole spike protein and its two constitutive parts, the S1 and S2 subunits. This contrasts with others who have focused on generating responses to the RBD region. An equine polyclonal preparation using the RBD of SARS-CoV-2 as the immunogen demonstrated neutralisation activity but without efficacy testing in a disease model (Zylberman et al., 2020). Similarly, genetically-modified pigs have been used to generate polyclonal glyco-humanised antibodies to develop a candidate product named 'XAV-19' which is being assessed in phase 2 trials, but similar to the equine preparation were immunised with only the RBD (Gaborit et al., 2021). Whilst RBD-specific antibodies have been demonstrated to be immunodominant in SARS-CoV-2 infection (Premkumar et al., 2020), antibodies which bind the S1 subunit outside of the RBD have also been shown to confer neutralising capacity (Chi et al., 2020; Jiang et al., 2020). Therefore, our approach also covers the areas outside of the RBD.

Antibody-based therapeutics suffer the risk of mutational escape of the target antigen, such as spike protein (Li et al., 2020). Studies have demonstrated that SARS-CoV-2 variants with mutations in the RBD can be readily selected (Weisblum et al., 2020). For monoclonal antibodies, this can be overcome by use of noncompeting antibodies (Baum et al., 2020), but the approach of targeting a broad area of the spike protein with polyclonal sera reduces mutational escape risk even further. Indeed, given the rise of variants with mutations in the spike protein (Harvey et al., 2021) the outbreak will continue to present challenges for control, and even more so for those therapies which focus on only a few antigenic epitopes. Given that there are at least 18 monoclonal antibodies against SARS-CoV-2 spike protein that are in clinical trials (Kumar et al., 2021), mutational escape poses a real risk to their effectiveness.

After immunisation of sheep, the antibody titre was at the highest level at week 6 demonstrating the rapid turnaround times achievable with this approach. This is earlier to when sheep were immunised with an Ebola virus antigen where the antibody levels reached maximum levels after 10 weeks (Dowall et al., 2016). When antibodies were affinity-purified, their binding levels to the specific antigen were all

consistently increased, confirming removal of unspecific antibodies from the preparation. The three preparations all showed similar binding levels to their respective immunisation antigen but differences in functional activity. The full-length specimen demonstrated strong binding to the RBD and had the strongest neutralising activity against live Wuhan-like virus (Victoria) and Omicron BA.1 *in vitro*. Hamsters given this preparation also demonstrated a milder clinical disease, with a significant reduction in maximum weight loss and reduction in lung histopathology. However, whilst the S2 antibody did not bind to the RBD, it still exerted neutralising activity. Interestingly, hamsters receiving S2-specific antibodies showed the same significant protective effects seen with the full-length antibodies, but with additional parameters also being significantly improved compared to control animals, including reduction in viral RNA in pharyngeal swabs at day 8 and 9 post-challenge, reduction in RNA levels in lung tissue taken at necropsy, lower levels of pneumonia and a reduced pathology score in both the lung and nasal cavity. The observation of S2-specific antibodies demonstrating neutralisation activity has been documented for SARS-CoV (Zeng et al., 2006). The S2 subunit contains structures that are critical for virus entry into cells, such as the fusion protein, and thus has conserved sequences which may explain the reactivity observed in some samples collected prior to the COVID-19 pandemic (Shrock et al., 2020). The S2-specific neutralisation may be due to several mechanisms, including the S2 subunit altering the structural change of the spike affecting the binding between the virus and its receptor which may prevent formation of a complementary surface between the two required for efficient neutralisation (Li et al., 2005). Other mechanisms include the S1 subunit and receptor binding being reversible so the virus may fail to stably dock without subsequent insertion of the fusion peptide into the host cell membrane functioned by the S2 subunit or simply due to the bulk of antibodies binding the S2 region hindering binding to the receptor (Zeng et al., 2006).

We report two animals which underwent antibody administration via the intraperitoneal route which did not translate into increased levels of circulating antibody in the blood. These animals were maintained in the dataset and analysis due to undergoing all procedures as planned and no substantial reason for exclusion outside of the subsequent measurement of antibody levels. It is not known why the antibody failed to enter the circulation. Using the intravenous route, which is the likely delivery route for use in human administration, is possible in small animal models but requires either very small samples being delivered or catheterisation of animals (Dowall et al., 2013).

In providing interim recommendations on assessing the effectiveness of convalescent plasma therapy, the Association for the Advancement of Blood & Biotherapies (AABB) indicate that the two most important factors are the quality of the product, as measured by neutralising antibody titre, and the disease state of the patients (Cohn et al., 2021). Our findings that the antibodies raised against the S2 subunit which were not highly neutralising and did not bind to the RBD demonstrate that other mechanisms are also involved in protective antibody function. Antibodies which do not neutralise may allow the virus-antibody complex to enter cells via endocytosis where other humoral effector functions may be performed such as antibody-dependent cell-mediated cytotoxicity (ADCC), antibody-mediated phagocytosis, aggregation and potentially immune activation (Excler et al., 2014; Mayr et al., 2017). Our results demonstrated S2 antibody binding to complement, and this activation of the complement system may aid in opsonophagocytosis or induce viral aggregation which can reduce virus levels (Santiesteban-Lores et al., 2021).

In addition to testing as a prophylactic, we also assessed giving the affinity-purified full-length spike Ab 3 days post-challenge to look at therapeutic effect. This timepoint was chosen due to clinical signs first being present in infected hamsters at this timepoint (Dowall et al., 2021). In humans, convalescent plasma has shown clinical benefit when used within 72 h from the onset of symptoms (Joyner et al., 2021; Libster et al., 2021). However, the disease progression in hamsters occurs over a shorter timeframe to disease observed in humans, with weight loss reversed after 6 days and live virus being detected in swabs until day 4 (Sia et al., 2020). To fully assess the prophylactic properties of the antibodies, earlier timepoints should be considered.

One issue with antibodies against SARS-CoV-2, whether induced through vaccination or with direct delivery, is the risk of antibody-dependent enhancement (ADE) as has been reported with SARS-CoV and MERS-CoV (Wen et al., 2020). A common mechanism of ADE is that the antibody promotes entry into host cells through the Fc receptor and complement receptor. Given that these antibodies are raised in sheep, this is reduced by no human Fc receptor being present. However, the risks could be further mitigated by further refinement of the antibodies into Fab or F(ab)2 fragments.

Whilst there are many vaccines for COVID-19, this may not be an option for immunocompromised and vulnerable populations where effective therapies are needed, particularly due to being prone to more severe COVID-19 (Focosi and Franchini 2021). Therefore, the results reported within presents an additional avenue applicable for both the current COVID-19 pandemic and future infectious disease threats.

Funding

This research was funded jointly by the National Institute for Health Research (NIHR) and the UK Research and Innovate (UKRI) through the COVID-19 Rapid Response Call for a project on ‘Development of an ovine polyclonal immunoglobulin therapy against COVID-19’ (Ref MC_PC_19077).

Declaration of competing interest

The authors declare the following financial interests/personal relationships which may be considered as potential competing interests: Sandra Smith and Neville Pope are employees of International Therapeutic Proteins Ltd. Gareth Humphries and Holger Schuhmann are employees of the Native Antigen Company. All other authors declare no known competing financial interests or personal relationships that could have appeared to influence the work reported in this paper.

Acknowledgements

The authors gratefully acknowledge the support from the Biological Investigations Group, Medical Interventions Group and Virology & Pathogenesis Group at UKHSA, Porton. The views expressed in this article are those of the authors and not necessarily those of the employing institutes or the funding bodies.

Appendix A. Supplementary data

Supplementary data to this article can be found online at https://doi.org/10.1016/j.ihjccr.2022.05.001.

References

Alexander, F., Brunt, E., Humphries, H., Cavell, B., Leung, S., Allen, L., Halkerston, R., Lesne, E., Penn, E., Thomas, S., Gorringe, A., Taylor, S., 2022. Generation of a universal human complement source by large-scale depletion of IgG and IgM from pooled human plasma. Methods Mol. Biol. 2414, 341–362.

Baum, A., Fulton, B.O., Wloga, E., Copin, R., Pascal, K.E., Russo, V., Giordano, S., Lanza, K., Negron, N., Ni, M., Wei, Y., Atwal, G.S., Murphy, A.J., Stahl, N., Yancopoulos, G.D., Kyratsous, C.A., 2020. Antibody cocktail to SARS-CoV-2 spike protein prevents rapid mutational escape seen with individual antibodies. Science 369 (6506), 1014–1018.

Belouzard, S., Millet, J.K., Licitra, B.N., Whittaker, G.R., 2012. Mechanisms of coronavirus cell entry mediated by the viral spike protein. Viruses 4 (6), 1011–1033.

Bewley, K.R., Coombes, N.S., Gagnon, L., McInroy, L., Baker, N., Shaik, I., St-Jean, J.R., St-Amant, N., Buttigieg, K.R., Humphries, H.E., Godwin, K.J., Brunt, E., Allen, L., Leung, S., Brown, P.J., Penn, E.J., Thomas, K., Kulnis, G., Hallis, B., Carroll, M., Funnell, S., Charlton, S., 2021. Quantification of SARS-CoV-2 neutralizing antibody by wild-type plaque reduction neutralization, microneutralization and pseudotyped virus neutralization assays. Nat. Protoc. 16 (6), 3114–3140.

Brown, E.P., Licht, A.F., Dugast, A.S., Choi, I., Bailey-Kellogg, C., Alter, G., Ackerman, M. E., 2012. High-throughput, multiplexed IgG subclassing of antigen-specific antibodies from clinical samples. J. Immunol. Methods 386 (1–2), 117–123.
Caly, L., Druce, J., Roberts, J., Bond, K., Tran, T., Kostecki, R., Yoga, Y., Naughton, W., Taiaroa, G., Seemann, T., Schultz, M.B., Howden, B.P., Korman, T.M., Lewin, S.R., Williamson, D.A., Catton, M.G., 2020. Isolation and rapid sharing of the 2019 novel coronavirus (SARS-CoV-2) from the first patient diagnosed with COVID-19 in Australia. Med. J. Aust. 212 (10), 459–462.
Cao, W., Liu, X., Bai, T., Fan, H., Hong, K., Song, H., Han, Y., Lin, L., Ruan, L., Li, T., 2020. High-dose intravenous immunoglobulin as a therapeutic option for deteriorating patients with coronavirus disease 2019. Open Forum Infect. Dis. 7 (3) ofaa102.
Chi, X., Yan, R., Zhang, J., Zhang, G., Zhang, Y., Hao, M., Zhang, Z., Fan, P., Dong, Y., Yang, Y., Chen, Z., Guo, Y., Zhang, J., Li, Y., Song, X., Chen, Y., Xia, L., Fu, L., Hou, L., Xu, J., Yu, C., Li, J., Zhou, Q., Chen, W., 2020. A neutralizing human antibody binds to the N-terminal domain of the Spike protein of SARS-CoV-2. Science 369 (6504), 650–655.
Cohn, C.S., Estcourt, L., Grossman, B.J., Pagano, M.B., Allen, E.S., Bloch, E.M., Casadevall, A., Devine, D.V., Dunbar, N.M., Foroutan, F., Gniadek, T.J., Goel, R., Gorlin, J., Joyner, M.J., Metcalf, R.A., Raval, J.S., Rice, T.W., Shaz, B.H., Vassallo, R. R., Winters, J.L., Beaudoin, G., Tobian, A.A.R., 2021. COVID-19 convalescent plasma: interim recommendations from the AABB. Transfusion 61 (4), 1313–1323.
Cucinotta, D., Vanelli, M., 2020. WHO declares COVID-19 a pandemic. Acta Biomed. 91 (1), 157–160.
Dowall, S., Salguerio, F.J., Wiblin, N., Fotheringham, S., Hatch, G., Parks, S., Gowan, K., Harris, D., Carnell, O., Fell, R., Watson, R., Graham, V., Gooch, K., Hall, Y., Mizen, S., Hewson, R., 2021a. Development of a hamster natural transmission model of SARS-CoV-2 infection. Viruses 13, 2251.
Dowall, S., Salguero, F.J., Wiblin, N., Fotheringham, S., Hatch, G., Parks, S., Gowan, K., Harris, D., Carnell, O., Fell, R., Watson, R., Graham, V., Gooch, K., Hall, Y., Mizen, S., Hewson, R., 2021b. Development of a hamster natural transmission model of SARS-CoV-2 infection. Viruses 13 (11).
Dowall, S., Taylor, I., Yeates, P., Smith, L., Rule, A., Easterbrook, L., Bruce, C., Cook, N., Corbin-Lickfett, K., Empig, C., Schlunegger, K., Graham, V., Dennis, M., Hewson, R., 2013. Catheterized Guinea pigs infected with Ebola Zaire virus allows safer sequential sampling to determine the pharmacokinetic profile of a phosphatidylserine-targeting monoclonal antibody. Antivir. Res. 97 (2), 108–111.
Dowall, S.D., Bosworth, A., Rayner, E., Taylor, I., Landon, J., Cameron, I., Coxon, R., Al Abdulla, I., Graham, V.A., Hall, G., Kobinger, G., Hewson, R., Carroll, M.W., 2016a. Post-exposure treatment of Ebola virus disease in Guinea pigs using EBOTAb, an ovine antibody-based therapeutic. Sci. Rep. 6, 30497.
Dowall, S.D., Callan, J., Zeltina, A., Al-Abdulla, I., Strecker, T., Fehling, S.K., Krahling, V., Bosworth, A., Rayner, E., Taylor, I., Charlton, S., Landon, J., Cameron, I., Hewson, R., Nasidi, A., Bowden, T.A., Carroll, M.W., 2016b. Development of a cost-effective ovine polyclonal antibody-based product, EBOTAb, to treat Ebola virus infection. J. Infect. Dis. 213 (7), 1124–1133.
Dowall, S.D., Jacquot, F., Landon, J., Rayner, E., Hall, G., Carbonnelle, C., Raoul, H., Pannetier, D., Cameron, I., Coxon, R., Al Abdulla, I., Hewson, R., Carroll, M.W., 2017. Post-exposure treatment of non-human primates lethally infected with Ebola virus with EBOTAb, a purified ovine IgG product. Sci. Rep. 7 (1), 4099.
Excler, J.L., Ake, J., Robb, M.L., Kim, J.H., Plotkin, S.A., 2014. Nonneutralizing functional antibodies: a new "old" paradigm for HIV vaccines. Clin. Vaccine Immunol. 21 (8), 1023–1036.
Focosi, D., Franchini, M., 2021. Potential use of convalescent plasma for SARS-CoV-2 prophylaxis and treatment in immunocompromised and vulnerable populations. Expert Rev. Vaccines 1–8.
Gaborit, B., Vanhove, B., Vibet, M.A., Le Thuaut, A., Lacombe, K., Dubee, V., Ader, F., Ferre, V., Vicaut, E., Orain, J., Le Bras, M., Omnes, A., Berly, L., Jobert, A., Morineau-Le Houssine, P., Botturi, K., Josien, R., Flet, L., Degauque, N., Brouard, S., Duvaux, O., Poinas, A., Raffi, F., group, P.s., 2021. Evaluation of the safety and efficacy of XAV-19 in patients with COVID-19-induced moderate pneumonia: study protocol for a randomized, double-blinded, placebo-controlled phase 2 (2a and 2b) trial. Trials 22 (1), 199.
Gutierrez, J.M., Leon, G., Lomonte, B., Angulo, Y., 2011. Antivenoms for snakebite envenomings. Inflamm. Allergy - Drug Targets 10 (5), 369–380.
Harvey, W.T., Carabelli, A.M., Jackson, B., Gupta, R.K., Thomson, E.C., Harrison, E.M., Ludden, C., Reeve, R., Rambaut, A., Consortium, C.-G.U., Peacock, S.J., Robertson, D.L., 2021. SARS-CoV-2 variants, spike mutations and immune escape. Nat. Rev. Microbiol. 19 (7), 409–424.
Haurum, J.S., 2006. Recombinant polyclonal antibodies: the next generation of antibody therapeutics? Drug Discov. Today 11 (13–14), 655–660.
Jiang, S., Hillyer, C., Du, L., 2020. Neutralizing antibodies against SARS-CoV-2 and other human coronaviruses. Trends Immunol. 41 (5), 355–359.
Joyner, M.J., Carter, R.E., Senefeld, J.W., Klassen, S.A., Mills, J.R., Johnson, P.W., Theel, E.S., Wiggins, C.C., Bruno, K.A., Klompas, A.M., Lesser, E.R., Kunze, K.L., Sexton, M.A., Diaz Soto, J.C., Baker, S.E., Shepherd, J.R.A., van Helmond, N., Verdun, N.C., Marks, P., van Buskirk, C.M., Winters, J.L., Stubbs, J.R., Rea, R.F., Hodge, D.O., Herasevich, V., Whelan, E.R., Clayburn, A.J., Larson, K.F., Ripoll, J.G., Andersen, K.J., Buras, M.R., Vogt, M.N.P., Dennis, J.J., Regimbal, R.J., Bauer, P.R., Blair, J.E., Paneth, N.S., Fairweather, D., Wright, R.S., Casadevall, A., 2021. Convalescent plasma antibody levels and the risk of death from covid-19. N. Engl. J. Med. 384 (11), 1015–1027.
Kim, J.H., Marks, F., Clemens, J.D., 2021. Looking beyond COVID-19 vaccine phase 3 trials. Nat. Med. 27 (2), 205–211.
Kumar, D., Gauthami, S., Bayry, J., Kaveri, S.V., Hegde, N.R., 2021. Antibody therapy: from diphtheria to cancer, COVID-19, and beyond. Monoclon. Antibodies Immunodiagn. Immunother. 40 (2), 36–49.
Lan, J., Ge, J., Yu, J., Shan, S., Zhou, H., Fan, S., Zhang, Q., Shi, X., Wang, Q., Zhang, L., Wang, X., 2020. Structure of the SARS-CoV-2 spike receptor-binding domain bound to the ACE2 receptor. Nature 581 (7807), 215–220.
Lewandowski, K., Xu, Y., Pullan, S.T., Lumley, S.F., Foster, D., Sanderson, N., Vaughan, A., Morgan, M., Bright, N., Kavanagh, J., Vipond, R., Carroll, M., Marriott, A.C., Gooch, K.E., Andersson, M., Jeffery, K., Peto, T.E.A., Crook, D.W., Walker, A.S., Matthews, P.C., 2019. Metagenomic Nanopore sequencing of influenza virus direct from clinical respiratory samples. J. Clin. Microbiol. 58 (1).
Li, F., Li, W., Farzan, M., Harrison, S.C., 2005. Structure of SARS coronavirus spike receptor-binding domain complexed with receptor. Science 309 (5742), 1864–1868.
Li, Q., Wu, J., Nie, J., Zhang, L., Hao, H., Liu, S., Zhao, C., Zhang, Q., Liu, H., Nie, L., Qin, H., Wang, M., Lu, Q., Li, X., Sun, Q., Liu, J., Zhang, L., Li, X., Huang, W., Wang, Y., 2020. The impact of mutations in SARS-CoV-2 spike on viral infectivity and antigenicity. Cell 182 (5), 1284–1294 e1289.
Libster, R., Perez Marc, G., Wappner, D., Coviello, S., Bianchi, A., Braem, V., Esteban, I., Caballero, M.T., Wood, C., Berrueta, M., Rondan, A., Lescano, G., Cruz, P., Ritou, Y., Fernandez Vina, V., Alvarez Paggi, D., Esperante, S., Ferreti, A., Ofman, G., Ciganda, A., Rodriguez, R., Lantos, J., Valentini, R., Itcovici, N., Hintze, A., Oyarvide, M.L., Etchegaray, C., Neira, A., Name, I., Alfonso, J., Lopez Castelo, R., Caruso, G., Rapelius, S., Alvez, F., Etchenique, F., Dimase, F., Alvarez, D., Aranda, S. S., Sanchez Yanotti, C., De Luca, J., Jares Baglivo, S., Laudanno, S., Nowogrodzki, F., Larrea, R., Silveyra, M., Leberzstein, G., Debonis, A., Molinos, J., Gonzalez, M., Perez, E., Kreplak, N., Pastor Arguello, S., Gibbons, L., Althabe, F., Bergel, E., Polack, F.P., Fundacion, I.-C.-G., 2021. Early high-titer plasma therapy to prevent severe covid-19 in older adults. N. Engl. J. Med. 384 (7), 610–618.
Mayr, L.M., Su, B., Moog, C., 2017. Non-Neutralizing antibodies directed against HIV and their functions. Front. Immunol. 8, 1590.
Ning, L., Abagna, H.B., Jiang, Q., Liu, S., Huang, J., 2021. Development and application of therapeutic antibodies against COVID-19. Int. J. Biol. Sci. 17 (6), 1486–1496.
Piechotta, V., Chai, K.L., Valk, S.J., Doree, C., Monsef, I., Wood, E.M., Lamikanra, A., Kimber, C., McQuilten, Z., So-Osman, C., Estcourt, L.J., Skoetz, N., 2020. Convalescent plasma or hyperimmune immunoglobulin for people with COVID-19: a living systematic review. Cochrane Database Syst. Rev. 7, CD013600.
Premkumar, L., Segovia-Chumbez, B., Jadi, R., Martinez, D.R., Raut, R., Markmann, A., Cornaby, C., Bartelt, L., Weiss, S., Park, Y., Edwards, C.E., Weimer, E., Scherer, E.M., Rouphael, N., Edupuganti, S., Weiskopf, D., Tse, L.V., Hou, Y.J., Margolis, D., Sette, A., Collins, M.H., Schmitz, J., Baric, R.S., de Silva, A.M., 2020. The receptor binding domain of the viral spike protein is an immunodominant and highly specific target of antibodies in SARS-CoV-2 patients. Sci. Immunol. 5 (48).
Redwan el, R.M., Fahmy, A., El Hanafy, A., Abd El-Baky, N., Sallam, S.M., 2009. Ovine anti-rabies antibody production and evaluation. Comp. Immunol. Microbiol. Infect. Dis. 32 (1), 9–19.
Redwan el, R.M., Khalil, A., El-Dardiri, Z.Z., 2005. Production and purification of ovine anti-tetanus antibody. Comp. Immunol. Microbiol. Infect. Dis. 28 (3), 167–176.
Santiesteban-Lores, L.E., Amamura, T.A., da Silva, T.F., Midon, L.M., Carneiro, M.C., Isaac, L., Bavia, L., 2021. A double edged-sword - the Complement System during SARS-CoV-2 infection. Life Sci. 272, 119245.
Shang, J., Wan, Y., Luo, C., Ye, G., Geng, Q., Auerbach, A., Li, F., 2020. Cell entry mechanisms of SARS-CoV-2. Proc. Natl. Acad. Sci. U. S. A. 117 (21), 11727–11734.
Shrock, E., Fujimura, E., Kula, T., Timms, R.T., Lee, I.H., Leng, Y., Robinson, M.L., Sie, B. M., Li, M.Z., Chen, Y., Logue, J., Zuiani, A., McCulloch, D., Lelis, F.J.N., Henson, S., Monaco, D.R., Travers, M., Habibi, S., Clarke, W.A., Caturegli, P., Laeyendecker, O., Piechocka-Trocha, A., Li, J.Z., Khatri, A., Chu, H.Y., Collection, M.C.-, Processing, T., Villani, A.C., Kays, K., Goldberg, M.B., Hacohen, N., Filbin, M.R., Yu, X.G., Walker, B.D., Wesemann, D.R., Larman, H.B., Lederer, J.A., Elledge, S.J., 2020. Viral epitope profiling of COVID-19 patients reveals cross-reactivity and correlates of severity. Science 370 (6520).
Sia, S.F., Yan, L.M., Chin, A.W.H., Fung, K., Choy, K.T., Wong, A.Y.L., Kaewpreedee, P., Perera, R., Poon, L.L.M., Nicholls, J.M., Peiris, M., Yen, H.L., 2020. Pathogenesis and transmission of SARS-CoV-2 in golden hamsters. Nature 583 (7818), 834–838.
Wang, Q., Zhang, Y., Wu, L., Niu, S., Song, C., Zhang, Z., Lu, G., Qiao, C., Hu, Y., Yuen, K. Y., Wang, Q., Zhou, H., Yan, J., Qi, J., 2020. Structural and functional basis of SARS-CoV-2 entry by using human ACE2. Cell 181 (4), 894–904 e899.
Weisblum, Y., Schmidt, F., Zhang, F., DaSilva, J., Poston, D., Lorenzi, J.C., Muecksch, F., Rutkowska, M., Hoffmann, H.H., Michailidis, E., Gaebler, C., Agudelo, M., Cho, A., Wang, Z., Gazumyan, A., Cipolla, M., Luchsinger, L., Hillyer, C.D., Caskey, M., Robbiani, D.F., Rice, C.M., Nussenzweig, M.C., Hatziioannou, T., Bieniasz, P.D., 2020. Escape from neutralizing antibodies by SARS-CoV-2 spike protein variants. Elife 9.
Wen, J., Cheng, Y., Ling, R., Dai, Y., Huang, B., Huang, W., Zhang, S., Jiang, Y., 2020. Antibody-dependent enhancement of coronavirus. Int. J. Infect. Dis. 100, 483–489.
Yao, H., Song, Y., Chen, Y., Wu, N., Xu, J., Sun, C., Zhang, J., Weng, T., Zhang, Z., Wu, Z., Cheng, L., Shi, D., Lu, X., Lei, J., Crispin, M., Shi, Y., Li, L., Li, S., 2020. Molecular architecture of the SARS-CoV-2 virus. Cell 183 (3), 730–738 e713.
Zeng, F., Hon, C.C., Yip, C.W., Law, K.M., Yeung, Y.S., Chan, K.H., Malik Peiris, J.S., Leung, F.C., 2006. Quantitative comparison of the efficiency of antibodies against S1 and S2 subunit of SARS coronavirus spike protein in virus neutralization and blocking of receptor binding: implications for the functional roles of S2 subunit. FEBS Lett. 580 (24), 5612–5620.
Zylberman, V., Sanguineti, S., Pontoriero, A.V., Higa, S.V., Cerutti, M.L., Morrone Seijo, S.M., Pardo, R., Munoz, L., Acuna Intrieri, M.E., Alzogaray, V.A., Avaro, M.M., Benedetti, E., Berguer, P.M., Bocanera, L., Bukata, L., Bustelo, M.S., Campos, A.M., Colonna, M., Correa, E., Cragnaz, L., Dattero, M.E., Dellafiore, M., Foscaldi, S.,

Gonzalez, J.V., Guerra, L.L., Klinke, S., Labanda, M.S., Lauche, C., Lopez, J.C., Martinez, A.M., Otero, L.H., Peyric, E.H., Ponziani, P.F., Ramondino, R., Rinaldi, J., Rodriguez, S., Russo, J.E., Russo, M.L., Saavedra, S.L., Seigelchifer, M., Sosa, S., Vilarino, C., Lopez Biscayart, P., Corley, E., Spatz, L., Baumeister, E.G., Goldbaum, F. A., 2020. Development of a hyperimmune equine serum therapy for COVID-19 in Argentina. Medicina 80 (Suppl. 3), 1–6.